THE JOURNAL OF PHYSICAL CHEMISTRY C

Article

pubs.acs.org/JPCC

Dimensional Dependence of the Optical Absorption Band Edge of TiO_2 Nanotube Arrays beyond the Quantum Effect

Ahmed Al-Haddad,[†,‡] Zhijie Wang,[†,§] Rui Xu,[†] Haoyuan Qi,[∥] Ranjith Vellacheri,[†] Ute Kaiser,[∥] and Yong Lei*[,†]

[†]Institute for Physics and IMN MacroNano, Ilmenau University of Technology, Professor Schmidt Strasse 26, 98693 Ilmenau, Germany

[‡]Department of Physics, College of Science, University of Al-Mustansiryah, Baghdad, Iraq

[§]Key Laboratory of Semiconductor Materials Science, Institute of Semiconductors, Chinese Academy of Sciences, Beijing, 100083, People's Republic of China

[∥]Central Facility of Electron Microscopy, Electron Microscopy Group of Materials Science, University of Ulm, Albert Einstein Allee 11, 89081 Ulm, Germany

Supporting Information

ABSTRACT: Instead of investigating the quantum effect that influences the absorption band edge of TiO_2 nanostructures, herein we report that geometrical parameters can also be utilized to manipulate the optical band gap of the TiO_2 nanotube arrays. Hexagonal arrays of TiO_2 nanotubes with an excellent crystalline quality were fabricated by techniques combining anodic aluminum oxide templates and atomic layer deposition. Through absorption spectroscopic analysis we observed that the optical absorption band edge of the TiO_2 nanotube arrays exhibited a red shift as the diameter of the nanotube was tuned to be larger and the distance between two nanotubes became smaller accordingly, while the wall thickness of the nanotube was kept constant. Subsequent finite-difference time-domain simulations supported the observation from theoretical aspect and revealed a large near-field enhancement around the outer space of the nanotubes for the arrays with densely distributed nanotubes when the corresponding arrays were exposed to the illuminations. Thus, this paper provides a new perspective for the shift of the optical band gap, which is of great significance to the research in photoelectronics.

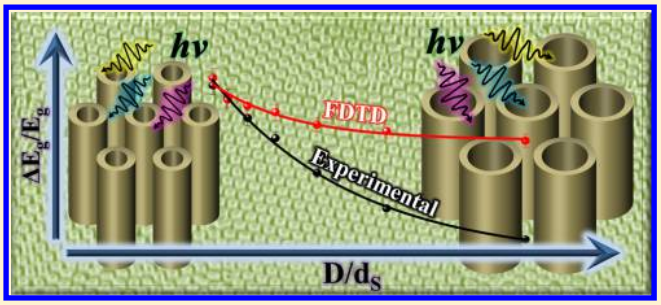

INTRODUCTION

The unique optical properties of semiconductor nanostructures have been extensively studied in the aspect of quantum confinement effects: when the dimensions of semiconductors are put at or below the characteristic size like exciton Bohr radius, the band gap becomes larger in comparison with the relevant bulk material, followed by a blue shift of the optical absorption onset. Such phenomenon is caused by localization of electrons and holes in a confined space that results in observable quantization of the energy levels of the electrons.[1−3] In this case, the optical properties of nanomaterials present a series of features that the bulk materials do not possess and have been widely applied in biomedicine,[4−6] sensors,[7] photonics,[8,9] and photovoltaics.[8,10] However, other geometrical factors excluding the quantum effects that influence the optical band gap of semiconductors are rarely reported.[11,12]

These days, the development of technologies for precisely controlling morphological parameters of nanostructures and the corresponding arrays enables us with sufficient approaches to turn back to reexamine the renowned optical band gap shift of semiconductors. Specifically, the technique based on anodic aluminum oxide (AAO) template has been proven to be one of the most popular methodologies to fabricate nanostructure arrays with perfectly manipulatable morphologies, owing to the advantages in low cost, easy fabrication, and high manipulation.[13−16] Accordingly, a large diversity of nanostructure arrays, including nanopores, nanodots, nanorods, nanotubes, and even the nanocones, has been realized.[13−22]

In consideration of the attractive property of TiO_2 that has been broadly utilized in dye-sensitized solar cells,[23,24] photocatalysts,[25] and photonics,[26,27] in this paper, we focus on the optical band gap modulation of TiO_2 nanotube arrays which were fabricated by the approach combining anodic aluminum oxide templates and atomic layer deposition (ALD). The subsequent absorption spectroscopic measurements demonstrated that the absorption band edge of the arrays exhibited a red shift when we tuned the diameter bigger and kept the wall thickness (W_t) of TiO_2 nanotube arrays constant. Finite-

Received: March 19, 2015
Revised: June 2, 2015

DOI: 10.1021/acs.jpcc.5b02665
J. Phys. Chem. C XXXX, XXX, XXX−XXX

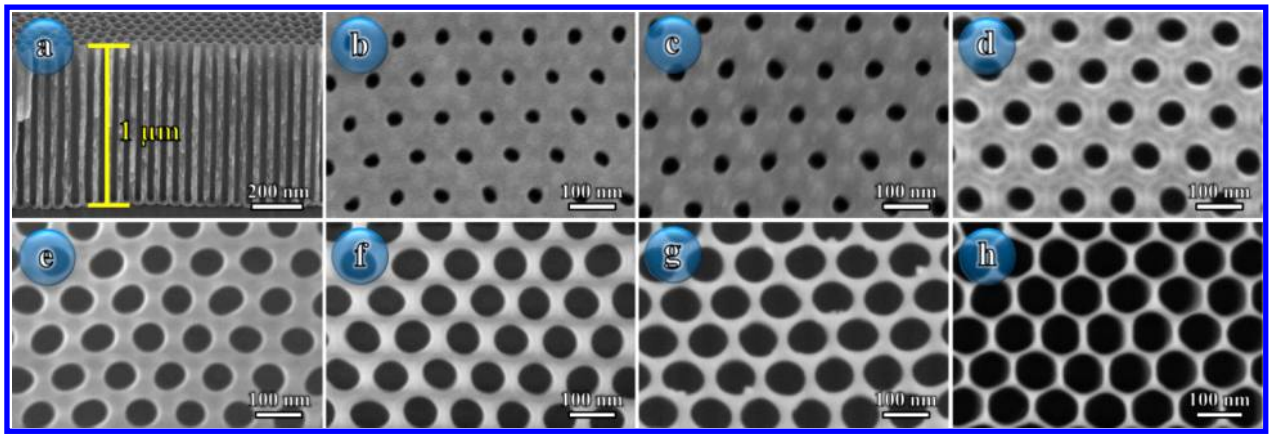

Figure 1. SEM images of the prepared AAO templates. (a) Cross-sectional image of AAO prepared by anodizing aluminum foil for 25 min at 7 °C. The fabricated samples have different pore diameters as well as interpore distances: (b) D = 30 nm, d_S = 80 nm; (c) D = 40 nm, d_S = 70 nm; (d) D = 50 nm, d_S = 60 nm; (e) D = 60 nm, d_S = 50 nm; (f) D = 70 nm, d_S = 40 nm; (g) D = 80 nm, d_S = 30 nm; (h) D = 90 nm, d_S = 20 nm.

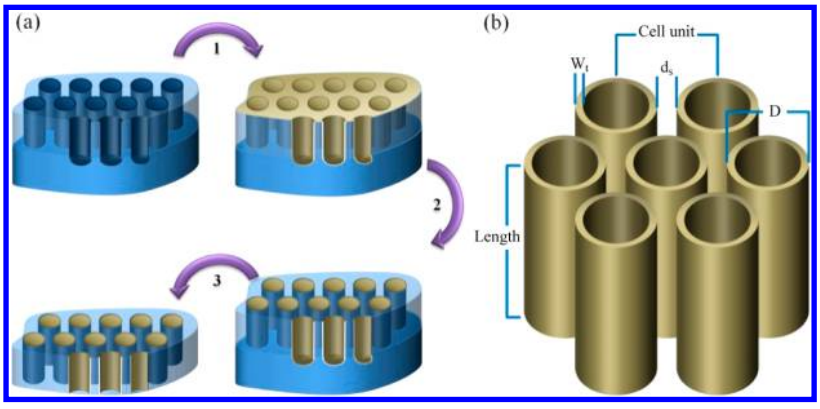

Figure 2. Schematic diagram of (a) preparation procedures of TiO_2 nanotube arrays: (1) TiO_2 deposition via ALD, (2) removing the surface layer of TiO_2 by argon ion milling, (3) removing aluminum in the backside. (b) Geometric illustration of the hexagonal nanotube arrays.

difference time-domain (FDTD) simulations supported the observations and illustrated a large near-field enhancement around the outer space of the nanotubes as we manipulated the distance between two nanotubes to a small value. Therefore, this paper offers an alternative possibility to tune the optical band gap of nanostructure arrays without concerning quantum confinement effects.

RESULTS AND DISCUSSION

The geometrical modulation of the TiO_2 nanotubes arrays begins with the precise tuning of the AAO templates. Figure 1 shows scanning electron microscopy (SEM) images of the AAO templates with a series of diameters (D: 30, 40, 50, 60, 70, 80, and 90 nm) and interpore distances (the distance between the edges of two neighbor pores, d_S: 80, 70, 60, 50, 40, 30, and 20 nm). The length is controlled as 1 μm by choosing the same anodization time for the samples as shown in Figure 1a. All these templates exhibit a uniform porous profile and perfectly ordered pore distribution, supplying us a good platform to fabricate well-controlled TiO_2 nanotube arrays.

The subsequent procedure for attaining TiO_2 nanotube arrays is depicted as the schematic in Figure 2a. Procedure 1 represents the growth of TiO_2 in AAO templates by the ALD method, and 200 cycles of deposition result in a thickness of 9.2 nm. Herein, we keep the samples with the same thickness to focus on the other factors and rule out the impact of quantum confinement effects. Procedure 2 describes the removing of the TiO_2 surface layer by argon ion milling, which is necessary to make the nanotube with a uniform pore size and to remove the two-dimensional (2-D) layer of TiO_2 from the surface. Procedure 3 shows the removing of aluminum in the backside to facilitate the optical absorption measurements. Finally, well-ordered TiO_2 nanotube arrays are prepared and schematically shown in Figure 2b, where the distribution of the nanotubes is purposely depicted to be hexagonal to match the real samples and FDTD simulation parameters.

Particularly in the procedure of ALD deposition, temperature was controlled at 250 °C. After deposition of the initial 40 cycles, the samples were purposely annealed at 480 °C for 1 h to improve the crystalline quality. The resultant 1.84 nm thick layer was utilized as the seed layer for the growth of the rest of the 160 cycles. Figure 3a shows the representative SEM images of the TiO_2 nanotube array in the AAO template after Ar ion milling. The entire AAO pores surface is covered by a thin layer of TiO_2. To check the infiltration of TiO_2 to pores, we have resolved different regions of the image: the top view and cross-sectional view near the top and the bottom of the array. All these images illustrate a uniform TiO_2 thickness running through the entire pores, indicative of a great advantage of the ALD technique to grow thin film uniformly without concerning the roughness of the substrates. After AAO template removal by soaking the samples in acidic solution, freestanding nanotubes arrays have also been attained even in a large scale as shown in Figure 3b.

DOI: 10.1021/acs.jpcc.5b02665
J. Phys. Chem. C XXXX, XXX, XXX−XXX

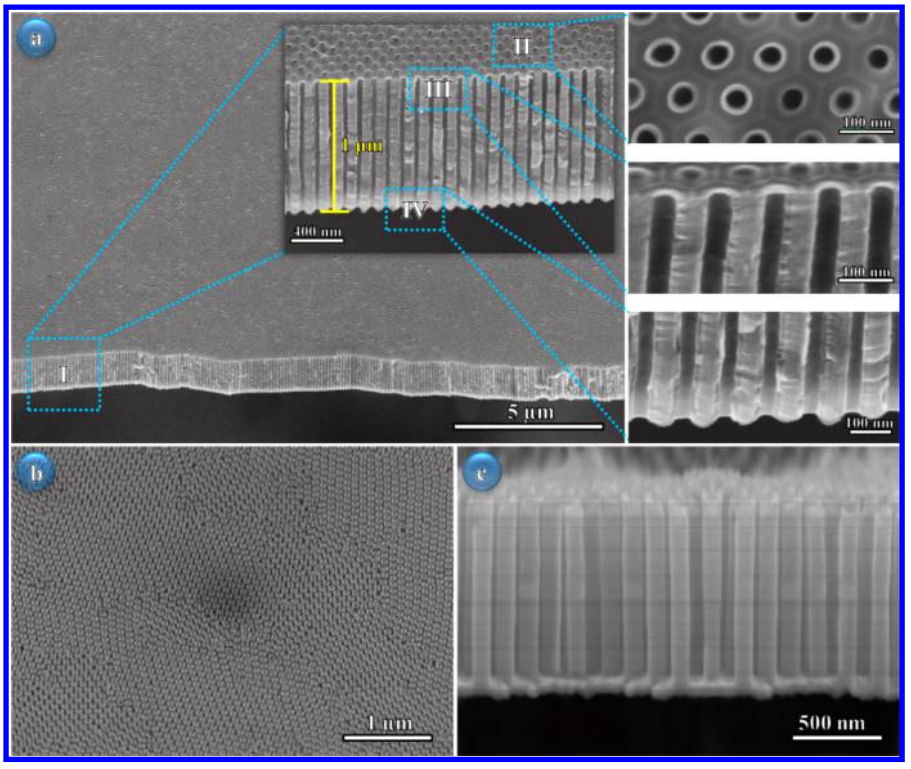

Figure 3. SEM micrographs of the prepared TiO_2 nanotube arrays. (a) Uniform TiO_2 layer covered the entire surface of AAO template pores; the magnified SEM image of region I shows the uniformity of the TiO_2 layer on the surface of AAO template pores, while the magnified SEM images of regions II, III, and IV show the uniform layer of TiO_2 at the top view and cross-sectional view around the top and the bottom of the arrays, respectively. (b) SEM image for the prepared TiO_2 nanotube arrays after removing the rest of the aluminum and AAO template. (c) Cross-sectional view of the freestanding TiO_2 nanotube arrays.

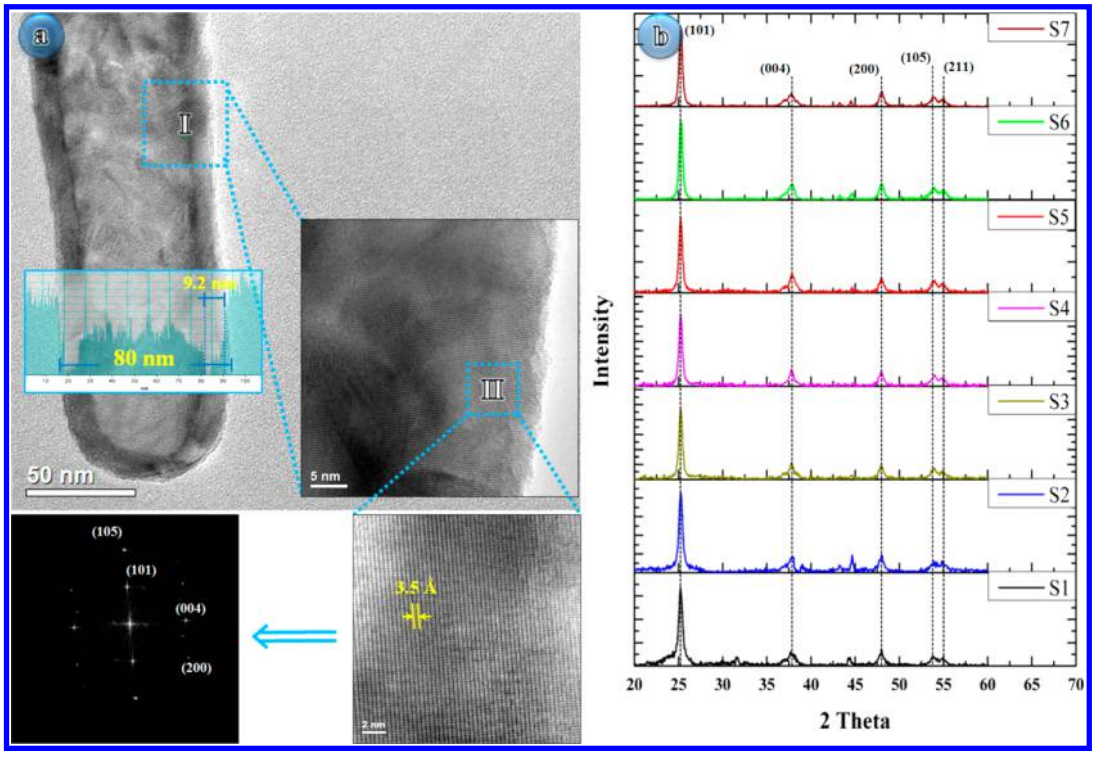

Figure 4. (a) TEM micrographs of a representative TiO_2 nanotube with thickness (W_t) of 9.2 nm and diameter (D) of 80 nm. The inset image of region II shows the crystalline TiO_2 nanostructure, and the HRTEM image of region II shows a single-crystalline structure of anatase TiO_2 nanostructure with a lattice spacing of 0.35 nm. SAED pattern is given on the left side. (b) XRD patterns showing the structure evolution of all the prepared samples of TiO_2 nanotube arrays (S1−S7).

DOI: 10.1021/acs.jpcc.5b02665
J. Phys. Chem. C XXXX, XXX, XXX−XXX

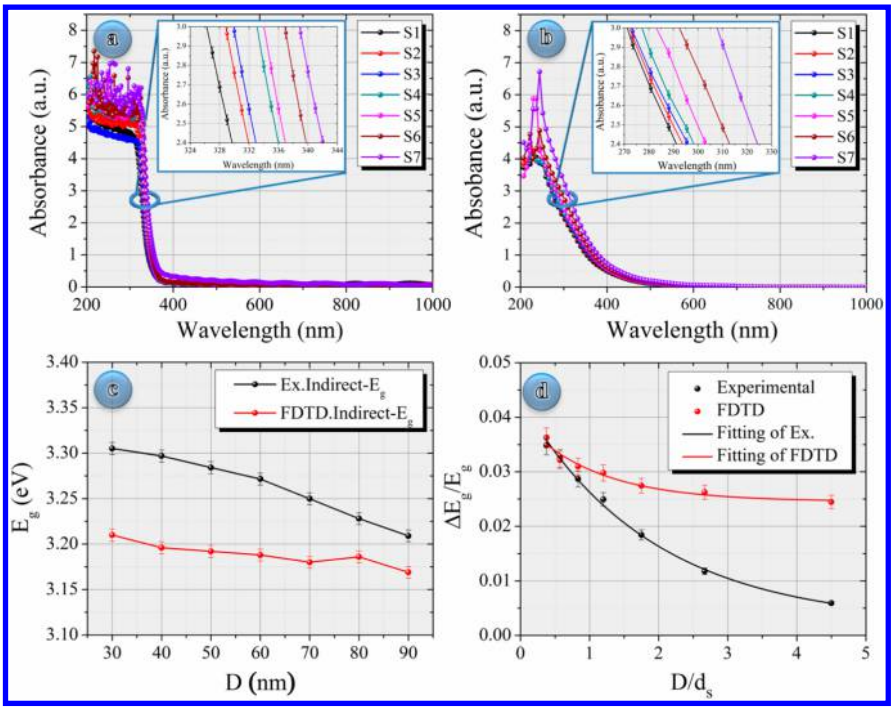

Figure 5. (a) Experimental absorbance spectra of the prepared TiO_2 nanotube arrays; the inset shows the red shift of the absorbance spectra for a specific region. (b) Simulated absorbance spectra of the proposed TiO_2 nanotube arrays using FDTD simulation; the inset shows the red shift of the absorbance spectra for a specific region. (c) Optical band gap of the TiO_2 nanotube arrays with different diameters. (d) Plots of $\Delta E_g/E_g$ vs D/d_S for experimental and FDTD simulated results.

Figure 4a shows the transmission electron microscopy (TEM) images for a representative TiO_2 nanotube. As we expect, the specific two-step ALD procedure results in a good crystalline quality for the grown nanotubes, which can be evidenced by the high-resolution TEM (HRTEM) image and selected area electron diffraction (SAED) pattern shown at the bottom. The crystal lattice fringes are clearly observed in the HRTEM image of region II, and the average distance between the adjacent lattice planes is 0.35 nm, corresponding to the (101) plane distance of anatase TiO_2. Liu et al.[28] have proven that the crystallinity of TiO_2 can be improved by controlling of the growth temperature to 400 °C. In our approach, such good crystalline quality of the as-grown material is obtained by two-step deposition without any additional annealing procedure for the second layer. During the deposition of the second layer at 400 °C, due to the slow ALD deposition process, TiO_2 is favorable to grow in an epitaxial way on the TiO_2 seed layer with high crystallinity. The thickness of the wall of nanotube is around 9.2 nm, and the diameter is around 80 nm, as gauged by the intensity profile across the nanotubes shown in the inset of Figure 4a. To investigate impact of the geometric parameters on the absorption properties of the nanotube arrays, we prepared the nanotube arrays with a constant wall thickness of 9.2 nm but different diameters, and the relevant TEM images are given in Supporting Information Figure S1, where the purposely controlled diameter is measured as 30, 40, 50, 60, 70, 80, and 90 nm, respectively. Figure 4b presents the X-ray diffraction (XRD) patterns of the series of prepared TiO_2 nanotube arrays with different diameters but same thickness, where a crystal structure of anatase TiO_2 could be easily concluded. The main diffraction peak belongs to the {101} planes, in good agreement with HRTEM analysis.

Figure 5a shows the absorbance spectra of TiO_2 nanotube arrays after subtracting the AAO template effect during the measurement. All these absorbance curves show an absorption band edge in the range of 350−400 nm, consistent with the absorbance spectrum of anatase TiO_2.[1,2] Though the thickness of these specimens is kept in the same value as 9.2 nm and the quantum effect should not render specificity among the resulting spectra, we can still observe an obvious red shift for the absorption edge according to the increase of diameters of the relevant nanotubes. In order to understand the interaction of photons with TiO_2 nanotube arrays more deeply, FDTD simulations were performed, and the simulated absorbance spectra for the same series of nanotube arrays are presented in Figure 5b. The same tendency of red shift with the widening of the nanotubes could also be prominently discerned in these simulated curves, revealing that there must be some other factors causing the shift of absorption edge beyond the quantum confinement effect. To make the observation more convincing, we have repeated the experiment and simulations in multiple times, and the according spectra with calculated error bars in the resolved range are shown as the insets of Figure 5, parts a and b. All of these spectra indicate a clear red-shifted tendency of optical absorbance onset of the TiO_2 nanotube arrays with the enlarging of the diameters.

More resolved spectra focused on the absorption edge in the form of Tauc plots are given in the Supporting Information Figure S2, and it can be clearly observed that the absorption onset is determined by the geometrical parameters like the diameters (D) and internal distance (d_S) of the nanotubes. Regarding that TiO_2 is classified as a standard indirect semiconductor, we preferentially use an indirect transition model, $\alpha = (h\nu - E_g)^2/h\nu$, to estimate the optical band gap values.[1,2] As exhibited in Figure 5c, the indirect optical band gap values from both the experimental and simulated data as the function of nanotube diameters are plotted. Though the estimated optical indirect band gap values from experiment and

DOI: 10.1021/acs.jpcc.5b02665
J. Phys. Chem. C XXXX, XXX, XXX−XXX

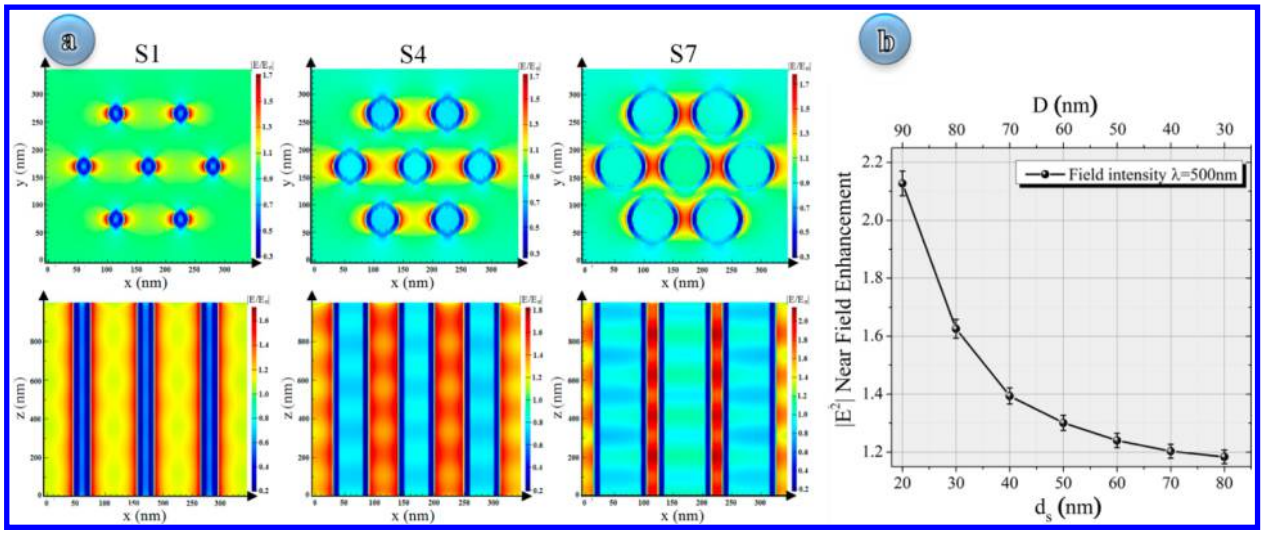

Figure 6. (a) FDTD simulation of E-field amplitude distribution under 500 nm illumination showing top and cross-sectional views of S1 (D = 30 nm, d_S = 80 nm), S4 (D = 60 nm, d_S = 50 nm), and S7 (D = 90 nm, d_S = 20 nm); the relevant results of other samples are given in Supporting Information Figure S4. (b) FDTD calculated $|E_x^2|$ enhancement at the top surface of TiO_2 nanotube arrays as a function of internal distance of TiO_2 nanotube under 500 nm illumination.

simulation present some deviations, probably because of the unavoidable roughness of the real samples, the narrowing of optical indirect band gap relevant to widening of the nanotube diameters for the two sets of data could be straightforwardly concluded. Moreover, considering the reversely proportional relationship of nanotube diameter and the internal distance between the nanotubes, we also present the plots of optical indirect band gap versus internal distance in Supporting Information Figure S3. These curves can confirm the observations in another aspect. To establish a universal analysis, we normalized the two geometrical parameters using D/d_S, and the corresponding correlations with indirect optical band gap change are shown in Figure 5d. With the increase of D/d_S, $\Delta E_g/E_g$ presents a decay feature that could be interpreted by a single-exponential model. Using the equation $\Delta E_g/E_g = Ae^{-\omega/\tau}$, where A is the constant and ω is the ratio of the nanotube diameter to internal distance of nanotubes ($\omega = D/d_S$), to fit the curves, decay constants (τ) for the experimental and FDTD simulated results are attained as 1.885 ± 0.122 and 1.067 ± 0.26, respectively. Though the two values show a little variation, probably due to the surface roughness from the real samples, we can still conclude that the geometric parameters cause the band gap shift without including the quantum effects.

As the size of the nanostructure decreases, indirect transitions could not explain all the findings, and direct transitions begin to be influential. Thus, we did the same analysis based on the direct transitions, and the according results are given in the Supporting Information. As demonstrated in Supporting Information Figure S3, like the indirect transitions, the direct optical band gap shows the same dependence on the nanotube diameters and distance between two nanotubes. In conclusion, all these data point out that the geometrical parameters could also cause an obvious change in optical band gap, apart from quantum effects. To investigate it more deeply, the interaction of the incident radiations with the nanostructure should be considered.

Figure 6 shows the simulated electric field distribution around the nanostructures in both top and cross-sectional views, when the samples are illuminated by the photons at 500 nm. The intensity decays as the spot moves from the surface of the nanotubes to the void space, implying that the interaction of photons and the nanostructure occurs on the outer surface of the nanotube, and the geometric property of such nanostructure could impact the interaction. By comparing the electric field of the samples with different geometrical parameters, it is easy to discover that the field intensity around the outer surface of nanotubes becomes higher as the diameter increases, implying a stronger coupling of the electric field for the sample with a smaller gap. This could be observed straightforwardly in the cross-sectional views of these structures by showing standing waves in between the nanotubes. Careful observations indicate a series of antinodes distributed along the longitudinal direction of the one side open tubes via a Kundt's tube experiment. These high-intensity spots are very similar to the plasmon hot spots on the surface of metallic nanoparticle arrays.[27] Though the electron density in TiO_2 is much lower than that in nanometals,[27,29] the interaction of incident radiations with the well-distributed TiO_2 nanotube arrays could indeed impact the corresponding absorption around the band gap edge, rendering a promising application in optical sensors.

It has been observed that, when the internal distance (d_S) between two TiO_2 nanotubes becomes smaller, the near-field coupling oscillation strength produces a strong confinement of the local electric field which enhances the spectroscopic signals. Such impact from the distributing of the nanotubes is consistent with the observations in nanometallic particle arrays. Jain et al.[30] derived a plasmon ruler equation for Au nanoparticle arrays and explained that, within the dipolar coupling model, the distance decay of plasmon coupling was independent of the nanoparticle shape, the metal type, and the medium of dielectric constant. To make a further analysis, we plot the curve for the near-field intensity enhancements ($|E_x^2|$)[31,32] at the top surface of the nanotubes versus the distance of the nanotubes. The $|E_x^2|$ presents a fast decay with the increase of the gap of the nanotubes, indicating that the coupling of the electric field becomes weak when the nanotube distribution is tuned sparse. Such weakened coupling could be responsible for the corresponding band gap shift of TiO_2 nanotube arrays.

DOI: 10.1021/acs.jpcc.5b02665
J. Phys. Chem. C XXXX, XXX, XXX−XXX

As to the band gap shift of TiO_2 nanotube arrays, Chang et al.[2] claim that such band gap shift could be realized by adjusting the wall thicknesses of TiO_2 nanotubes in the range of 2.7−37.8 nm, which is based on the conventional quantum confinement effect. However, our results indicate that the band gap shift can also be acquired only by adjusting the diameters and the distances between nanotubes; even these parameters are larger than the Bohr radius of TiO_2, and quantum effects are not responsible for this observation, since the thicknesses of these nanotubes are in the same value. We attribute this specific optical band gap shift to the interaction of the incident radiations with the highly ordered nanostructure arrays, and the tunability of the band gap is related to the strength of the near-field enhancement of light. Thus, this paper broadens the tuning range of optical properties of nanostructure arrays and the according possibilities for photoelectronic applications.

CONCLUSIONS

In summary, we have successfully prepared well-ordered TiO_2 nanotube arrays by combining ALD technology with an AAO template. The crystalline quality of deposited TiO_2 was enhanced using a two-step ALD procedure. By tuning the nanotube arrays with different diameters and internal distances but the same wall thickness, the resulting absorption band edge showed a red shift with the decrease of the internal distances. This phenomenon was proven by the FDTD simulation. The calculated decay constant of the optical band gap over the ratio of nanotube diameter/internal distance demonstrated that the tunability of band gap was related to the strength of the near-field enhancement of light. Thereby, this paper supplies a new perspective for the optical band gap shift of semiconductor nanostructure arrays.

EXPERIMENTAL SECTION

The AAO template was prepared by anodic oxidation of high-purity aluminum foil (99.999%) according to our previous reports.[13−15] The AAO template thickness and pores diameters were fixed by well controlling the time of anodization and pore widening processes. Seven samples of AAO with different diameters were placed inside the chamber of the ALD, followed by the increase of temperature to 250 °C. $TiCl_4$ and H_2O were selected as Ti and O_2 sources, and N_2 gas was used as both carrier gas and purge gas. The typical pulse time used to introduce the $TiCl_4$ and H_2O precursors was 0.1 s, and the N_2 purge time was 5 s. The initial depositing cycles were 40 cycles to generate a 1.84 nm TiO_2 continuous layer that covered the entire surface of template. Thereafter, samples were annealed inside the ALD chamber at 480 °C for 1 h to create a crystalline seed layer for next 160 cycles of TiO_2 deposition at 400 °C. The total deposition cycles were chosen as 200 cycles to produce a specific TiO_2 nanotube wall thickness (9.2 nm). The as-prepared TiO_2 nanotube arrays were examined using a scanning electron microscope (SEM, Hitachi S 4800) and transmission electron microscopes (Philips TECNAI and FEI Titan 80-300). X-ray diffraction (XRD, Siemens D5000) was utilized to analyze the crystal structure of the TiO_2 nanotubes. A UV−vis spectrometer (Varian) was adopted to measure the absorption characteristic of the TiO_2 nanotube arrays.

The optical properties of TiO_2 nanotube arrays were simulated using three-dimensional full-field finite difference time domain methods (Lumerical FDTD Solutions 8.9). The dielectric constants were obtained from a fit to the experimentally recorded refractive index data of the ALD-deposited TiO_2 thin films which were used in nanotubes fabrication. Broad-band linearly polarized plane waves were perpendicularly incident onto individual nanotube arrays with periodic in-plane boundary conditions. Seven TiO_2 nanotubes with the same geometric parameters as those in the real samples were used for all set of the simulations in a hexagonal geometry. Meshing size as small as 1 nm was used in the regions containing TiO_2, which was proven fine enough in convergence tests. The field vectors were monitored in three-dimensional grid points to extract transmittance spectra of TiO_2 nanotubes and to generate field distribution maps at wavelengths of interest.

ASSOCIATED CONTENT

Supporting Information

TEM images of the prepared TiO_2 nanotube arrays shown with the same wall thickness at different diameters, Tauc plots of indirect and direct optical band gap calculations, band gap as a function of internal distance of TiO_2 nanotubes, and FDTD simulation of E-field amplitude distribution for all the prepared samples. The Supporting Information is available free of charge on the ACS Publications website at DOI: 10.1021/acs.jpcc.5b02665.

AUTHOR INFORMATION

Corresponding Author

*E-mail: yong.lei@tu-ilmenau.de.

Notes

The authors declare no competing financial interest.

ACKNOWLEDGMENTS

Ahmed Al-Haddad would like to thank the German Academic Exchange Service (DAAD) for the Ph.D. fellowship. The authors acknowledge the financial support from the European Research Council (ThreeDsurface, 240144), BMBF (ZIK-3DNanoDevice, 03Z1MN11), BMBF (Meta-ZIK-BioLitho-Morphie, 03Z1M511), and Volkswagen-Stiftung (Herstellung funktionaler Oberflächen, I/83 984).

REFERENCES

(1) Serpone, N.; Lawless, D.; Khairutdinov, R. Size Effects on the Photophysical Properties of Colloidal Anatase TiO_2 Particles: Size Quantization Versus Direct Transitions in This Indirect Semiconductor? *J. Phys. Chem.* **1995**, *99*, 16646−16654.

(2) Chang, Y.-H.; Liu, C.-M.; Cheng, H.-E.; Chen, C. Effect of Geometric Nanostructures on the Absorption Edges of 1-D and 2-D TiO_2 Fabricated by Atomic Layer Deposition. *ACS Appl. Mater. Interfaces* **2013**, *5*, 3549−3555.

(3) Bavykin, D. V.; Gordeev, S. N.; Moskalenko, A. V.; Lapkin, A. A.; Walsh, F. C. Apparent Two-Dimensional Behavior of TiO_2 Nanotubes Revealed by Light Absorption and Luminescence. *J. Phys. Chem. B* **2005**, *109*, 8565−8569.

(4) Kono, K.; Takeda, K.; Li, X.; Yuba, E.; Harada, A.; Ozaki, T.; Mori, S. Dually Functionalized Dendrimers by Temperature-Sensitive Surface Modification and Gold Nanoparticle Loading for Biomedical Application. *RSC Adv.* **2014**, *4*, 27811−27819.

(5) Lewis, D. J.; Pikramenou, Z. Lanthanide-Coated Gold Nanoparticles for Biomedical Applications. *Coord. Chem. Rev.* **2014**, *273−274*, 213−225.

(6) Walkey, C. D.; Olsen, J. B.; Song, F.; Liu, R.; Guo, H.; Olsen, D. W. H.; Cohen, Y.; Emili, A.; Chan, W. C. Protein Corona Fingerprinting Predicts the Cellular Interaction of Gold and Silver Nanoparticles. *ACS Nano* **2014**, *8*, 2439−2455.

DOI: 10.1021/acs.jpcc.5b02665
J. Phys. Chem. C XXXX, XXX, XXX−XXX

(7) Liang, Y.-C.; Liao, W.-K.; Deng, X.-S. Synthesis and Substantially Enhanced Gas Sensing Sensitivity of Homogeneously Nanoscale Pd- and Au-Particle Decorated ZnO Nanostructures. *J. Alloys Compd.* **2014**, *599*, 87−92.
(8) Priolo, F.; Gregorkiewicz, T.; Galli, M.; Krauss, T. F. Silicon Nanostructures for Photonics and Photovoltaics. *Nat. Nanotechnol.* **2014**, *9*, 19−32.
(9) Hernández-Martínez, P. L.; Govorov, A. O.; Demir, H. V. Förster-Type Nonradiative Energy Transfer for Assemblies of Arrayed Nanostructures: Confinement Dimension vs Stacking Dimension. *J. Phys. Chem. C* **2014**, *118*, 4951−4958.
(10) Brongersma, M. L.; Cui, Y.; Fan, S. Light Management for Photovoltaics Using High-Index Nanostructures. *Nat. Mater.* **2014**, *13*, 451−460.
(11) Fan, H. J.; Werner, P.; Zacharias, M. Semiconductor Nanowires: From Self-Organization to Patterned Growth. *Small* **2006**, *2*, 700−717.
(12) Li, M.; Li, J. C. Size Effects on the Band-Gap of Semiconductor Compounds. *Mater. Lett.* **2006**, *60*, 2526−2529.
(13) Lei, Y.; Yang, S.; Wu, M.; Wilde, G. Surface Patterning Using Templates: Concept, Properties and Device Applications. *Chem. Soc. Rev.* **2011**, *40*, 1247−1258.
(14) Lei, Y.; Cai, W.; Wilde, G. Highly Ordered Nanostructures with Tunable Size, Shape And Properties: A New Way to Surface Nano-Patterning Using Ultra-Thin Alumina Masks. *Prog. Mater. Sci.* **2007**, *52*, 465−539.
(15) Wu, M.; Wen, L.; Lei, Y.; Ostendorp, S.; Chen, K.; Wilde, G. UTAM Surface Nano-Patterning in Fabricating Quantum-Sized Nanodots. *Small* **2010**, *6*, 695.
(16) Chang, Y.-H.; Liu, C.-M.; Chen, C.; Cheng, H.-E.; Lu, T.-C. The Differences in Optical Characteristics of TiO_2 and TiO_2/AAO Nanotube Arrays Fabricated by Atomic Layer Deposition. *J. Electrochem. Soc.* **2012**, *159*, K136−K140.
(17) Lei, Y.; Liang, C.; Wu, Y.; Zhang, L.; Mao, Y. Preparation of Highly Ordered Nanoporous Co Membranes Assembled by Small Quantum-Sized Co Particles. *J. Vac. Sci. Technol., B* **2001**, *19*, 1109−1114.
(18) Lei, Y.; Chim, W.; Zhang, Z.; Zhou, T.; Zhang, L.; Meng, G.; Phillipp, F. Ordered Nanoporous Nickel Films and Their Magnetic Properties. *Chem. Phys. Lett.* **2003**, *380*, 313.
(19) Chen, Z.; Lei, Y.; Chew, H.; Teo, L.; Choi, W.; Chim, W. Synthesis of Germanium Nanodots on Silicon Using an Anodic Alumina Membrane Mask. *J. Cryst. Growth* **2004**, *268*, 560.
(20) Zhan, Z.; Lei, Y. Sub-100-nm Nanoparticle Arrays with Perfect Ordering Tunable and Uniform Dimensions Fabricated by Combining Nanoimprinting with Ultrathin Alumina Membrane Technique. *ACS Nano* **2014**, *8*, 3862−3868.
(21) Wen, L.; Mi, Y.; Wang, C.; Fang, Y.; Grote, F.; Zhao, H.; Zhou, M.; Lei, Y. Cost-Effective Atomic Layer Deposition Synthesis of Pt Nanotube Arrays: Application for High Performance Supercapacitor. *Small* **2014**, *10*, 3162−3168.
(22) Zhao, S.; Roberge, H.; Yelon, A.; Veres, T. New Application of AAO Template: A Mold for Nanoring and Nanocone Arrays. *J. Am. Chem. Soc.* **2006**, *128*, 12352−12353.
(23) Shankar, K.; Mor, G. K.; Prakasam, H. E.; Yoriya, S.; Paulose, M.; Varghese, O. K.; Grimes, C. A. Highly-Ordered TiO_2 Nanotube Arrays up to 220 μm in Length: Use in Water Photoelectrolysis and Dye-Sensitized Solar Cells. *Nanotechnology* **2007**, *18*, 65707−65718.
(24) Zhang, M.; Wang, Y.-N.; Moulin, E.; Grützmacher, D.; Chien, C.-J.; Chang, P.-C.; Gao, X.; Carius, R.; Lu, J. G. Core−Shell CdTe−TiO_2 Nanostructured Solar Cell. *J. Mater. Chem.* **2012**, *22*, 10441−10443.
(25) Lin, H.; Huang, C.; Li, W.; Ni, C.; Shah, S.; Tseng, Y. Size Dependency Of Nanocrystalline TiO_2 on Its Optical Property and Photocatalytic Reactivity Exemplified by 2-Chlorophenol. *Appl. Catal., B* **2006**, *68*, 1−11.
(26) Kwon, D. H.; Kim, K. M.; Jang, J. H.; Jeon, J. M.; Lee, M. H.; Kim, G. H.; Li, X. S.; Park, G. S.; Lee, B.; Han, S.; et al. Atomic Structure of Conducting Nanofilaments in TiO_2 Resistive Switching Memory. *Nat. Nanotechnol.* **2010**, *5*, 148−153.
(27) Le, F.; Brandl, D. W.; Urzhumov, Y. A.; Wang, H.; Kundu, J.; Halas, N. J.; Aizpurua, J.; Nordlander, P. Metallic Nanoparticle Arrays: A Common Substrate for Both Surface-Enhanced Raman Scattering and Surface-Enhanced Infrared Absorption. *ACS Nano* **2008**, *2*, 707−718.
(28) Liu, C.-M.; Chen, C.; Cheng, H.-E. Growth Mechanism of TiO_2 Nanotube Arrays in Nanopores of Anodic Aluminum Oxide on Si Substrates by Atomic Layer Deposition. *J. Electrochem. Soc.* **2011**, *158*, K58−K63.
(29) Park, S. J.; Lee, J. P.; Jang, J. S.; Rhu, H.; Yu, H.; You, B. Y.; Kim, C. S.; Kim, K. J.; Cho, Y. J.; Baik, S.; et al. In Situ Control of Oxygen Vacancies in TiO_2 by Atomic Layer Deposition for Resistive Switching Devices. *Nanotechnology* **2013**, *24*, 295202−295213.
(30) Jain, P. K.; Huang, W.; El-Sayed, M. A. On the Universal Scaling Behavior of the Distance Decay of Plasmon Coupling in Metal Nanoparticle Pairs: A Plasmon Ruler Equation. *Nano Lett.* **2007**, *7*, 2080−2088.
(31) Crozier, K.; Sundaramurthy, A.; Kino, G.; Quate, C. Optical Antennas: Resonators for Local Field Enhancement. *J. Appl. Phys.* **2003**, *94*, 4632−4642.
(32) Sundaramurthy, A.; Crozier, K.; Kino, G.; Fromm, D.; Schuck, P.; Moerner, W. Field Enhancement and Gap-Dependent Resonance in A System Of Two Opposing Tip-to-Tip Au Nanotriangles. *Phys. Rev. B* **2005**, *72*, 165409−165415.

DOI: 10.1021/acs.jpcc.5b02665
J. Phys. Chem. C XXXX, XXX, XXX−XXX